A Study of M–X–BR_3 (M = Pt, Pd or Rh; X = Cl or I) Interactions in Square Planar Ambiphilic Ligand Complexes: Structural, Spectroscopic, Electrochemical and Computational Comparisons with Borane-Free Analogues

David J. H. Emslie,[a] Bradley E. Cowie,[a] Simon R. Oakley,[a] Natalie. L. Huk,[a] Hilary A. Jenkins,[b] Laura E. Harrington[b] and James F. Britten[b]*

[a] Department of Chemistry, McMaster University, 1280 Main Street West, Hamilton, ON, L8S 4M1, Canada. Fax: (905)-522-2509; Tel: (905)-525-9140 x 23307; E-mail: emslied@mcmaster.ca.

[b] McMaster Analytical X-Ray Diffraction Facility, Department of Chemistry, McMaster University, 1280 Main Street West, Hamilton, ON, L8S 4M1, Canada.

RECEIVED DATE

Abstract: Reaction of [$PtCl_2$(COD)] and [PtI_2(COD)] with 2,7-di-*tert*-butyl-5-diphenylboryl-4-diphenylphosphino-9,9-dimethylthioxanthene (**TXPB**) afforded square planar [$PtCl_2$(TXPB)] (**1B**) and [PtI_2(TXPB)] (**4B**), both of which were crystallographically characterized. X-ray quality crystals were also obtained for [$PdCl_2$(TXPB)] (**2B**; Emslie *et al. Organometallics*, **2008**, *27*, 5317) as **2B**·$2CH_2Cl_2$ and solvent-free **2B**. Both the chloro and iodo TXPB complexes exhibit metal–halide–borane bridging interactions similar to those in previously reported [RhCl(CO)(TXPB)] (**3B**) and [RhI(CO)(TXPB)] (**5B**) (Emslie *et al. Organometallics*, **2006**, *25*, 583 & *Inorg. Chem.* **2010**, *49*, 4060). To facilitate more detailed analysis of M–X–BR_3 (X = Cl and I) interactions, a borane-free analogue of the TXPB ligand, 2,7-di-*tert*-butyl-4-diphenylphosphino-9,9-dimethylthioxanthene (**TXPH**), was prepared, and reaction with [PtX_2(COD)] (X = Cl or I), [$PdCl_2$(COD)] and 0.5 [{$RhCl(CO)_2$}$_2$] provided square planar [$PtCl_2$(TXPH)] (**1H**), [$PdCl_2$(TXPH)] (**2H**), [RhCl(CO)(TXPH)] (**3H**) and [PtI_2(TXPH)] (**4H**). M–Cl–BR_3 and M–I–BR_3 bonding in **1B**-**5B** was then probed through the use of structural comparisons, IR and NMR spectroscopy, cyclic voltammetry, and DFT calculations (Slater-type orbitals, Mayer bond orders, Hirshfeld charges, fragment analysis, SCF deformation density isosurfaces, and energy decomposition analysis).

Introduction

Ambiphilic ligands are defined as those containing a Lewis acidic group in addition to one or more conventional donors capable of σ-donation to the metal (e.g. a phosphine or an amine). These ligands may be generated *in situ* on a metal, as is typically the case for tris(*N*-alkylimazolyl)boranes, or they may be isolated prior to metal coordination. The transition metal chemistry of group 13 Lewis acid-containing ambiphilic ligands has seen a surge of activity over the past decade, much of it directed towards the isolation and study of unusual metal–Lewis acid bonds where the Lewis acid is considered a zero-electron donor Z-type ligand.[1] However, studies focused on the development of cooperative reactivity involving a pendant group 13 Lewis acid have also been reported. These include: (1) pendant borane facilitated delivery of multiple hydride equivalents to a carbonyl ligand in $[Re(CO)_4\{PPh_2(CH_2)_2B(C_8H_{14})\}_2]^+$ (I in Figure 1), followed by spontaneous alkyl migration to form a C–C bond,[2] (2) rate enhancements for the dehydrogenative coupling of $PhSiH_3$ by [(Me-Ind)NiMe(PPh_3)] in the presence of $Me_2PCH_2AlMe_2$; the proposed intermediate in this reactivity is [(Me-Ind)NiMe($PMe_2CH_2AlMe_2$)] (II in Figure 1),[3] (3) propene and methane formation upon reaction of [Cp*$RhMe_2$($PMe_2CH_2AlMe_2$)] with ethylene at 50 °C; [Cp*$Rh^+Me(C_2H_4)(PMe_2CH_2AlMe_3^-)$] (III in Figure 1) was identified as an intermediate in this reaction,[4] (4) reaction of $Na[H_2B(mt)_2]$ (mt = *N*-methylimazolyl) with [RhCl(CS)(PPh_3)$_2$] to form [LRhH(PPh_3)] [IV in Figure 1; L = $\{H(mt)_2B\}(Ph_3P)C{=}S$], presumably *via* the intermediates [{κ^3-$H_2B(mt)_2$}Rh(CS)(PPh_3)] (V in Figure 1) and [{κ^3-$HB(mt)_2$}RhH(CS)(PPh_3)],[5] (5) reaction of [{κ^4-$B(mt^{tBu})_3$}NiCl] (VI in Figure 1; mt^{tBu} = *N*-*tert*-butylimazolyl)) with I_2 or $CHBr_3$ to form [{κ^3-$ClB(mt^{tBu})_3$}NiX] (VII in Figure 1; X = I or Br), and with XeF_2 to produce [{κ^3-$FB(mt^{tBu})_3$}NiCl],[6] and (6) Reaction of [Pd(TXPB)] (VIII in Figure 1; TXPB = 2,7-di-*tert*-butyl-5-diphenylboryl-4-diphenylphosphino-9,9-dimethylthioxanthene) with dibenzylidene-acetone (dba) to afford [Pd(dba)(TXPB)] (IX in Figure 1); a zwitterionic palladium(II) η^3-boratoxyallyl complex.[7]

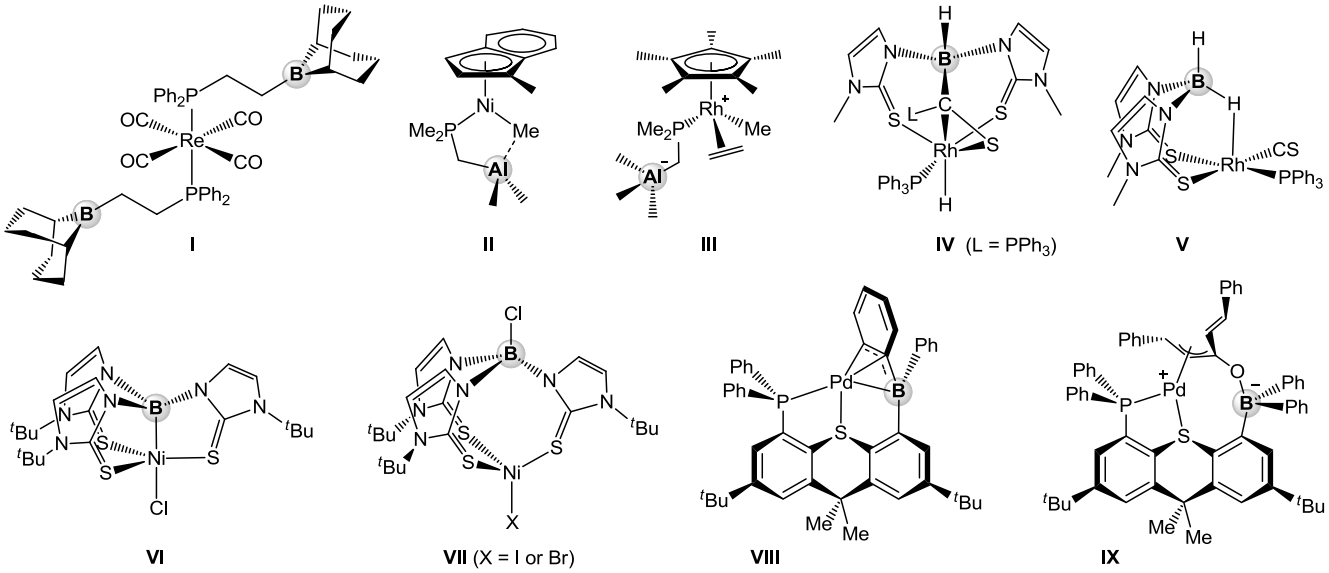

Figure 1. Selected reactants, proposed intermediates and products from reactions involving a pendant group 13 Lewis acid (the group 13 element is highlighted).

Previous research in the Emslie group has focused on late transition metal complexes of the phosphine-thiether-borane ambiphilic ligand, TXPB, and a range of complexes containing direct metal–borane or metal–ligand–borane interactions have been prepared, including compounds VIII and IX in Figure 1.[7,8,9] The current work probes the nature of halide ligand coordination by a pendant borane; in particular the extent to which the strength of metal–halide–borane (M–X–BR_3) interactions vary between chloro and iodo complexes, and the effect that borane coordination has on the metal–halide bond. Our interest in these features is twofold: (1) For late transition metal catalysis involving halide ligands, it is possible to envisage modified reaction cycles involving halide coordination or abstraction by a pendant borane. However, to allow rational progress in this direction, a more detailed understanding of metal–halide–borane interactions is desirable. (2) The potential exists for a pendant borane to effect pre-coordination or cooperative activation of organic substrates. However, due to the ubiquitous nature of chloro, bromo and iodo ligands throughout much of transition metal chemistry, it is desirable to

determine the extent to which coordination of halide co-ligands is likely to take place, potentially sequestering the pendant borane.

A previous publication reported the synthesis and structural characterization of [RhX(CO)(TXPB)] (X = F, Cl, Br and I) complexes, revealing short B–X distances in the chloro and bromo complexes, a long B–I interaction in the iodo complex, and halide abstraction by the borane in the fluoro complex.[8] This trend is in keeping with the soft nature of rhodium(I), the classification of organoboranes as moderately hard Lewis acids, and the decrease in halide hardness as group 17 is descended.[10] Herein we provide a more detailed analysis of M–X–BR_3 (M = Pt, Pd or Rh; X = Cl or I) bonding in [MX_2(TXPB)] and [MX(CO)(TXPB)] complexes through the use of crystallographic, spectroscopic, electrochemical and computational comparisons with borane-free TXPH ligand analogues (TXPH = 2,7-di-*tert*-butyl-4-diphenylphosphino-9,9-dimethylthioxanthene).

Results and Discussion

Platinum Dichloro and Diiodo Complexes of TXPB: Reaction of [$PtCl_2$(COD)] with 2,7-di-*tert*-butyl-5-diphenylboryl-4-diphenylphosphino-9,9-dimethylthioxanthene (TXPB)[7] afforded colourless [$PtCl_2$(TXPB)] (**1B**) in moderate yield (Scheme 1). The ^{31}P NMR signal at 32.5 ppm ($^1J_{P,Pt}$ = 3836 Hz) demonstrates platinum–phosphine coordination and the ^{11}B NMR signal at 3 ppm is characteristic of 4-coordinate boron. These data are consistent with square planar platinum ligated by the phosphine and thioether groups of TXPB and two chloride anions, with one chloride forming a strong bridging interaction to the borane unit of TXPB. Analogous M–Cl–B bridging interactions have been observed in the solid state structures of [RhCl(CO)(TXPB)] (**3B**) and [{PdCl(TXPB)}$_2$].[9]

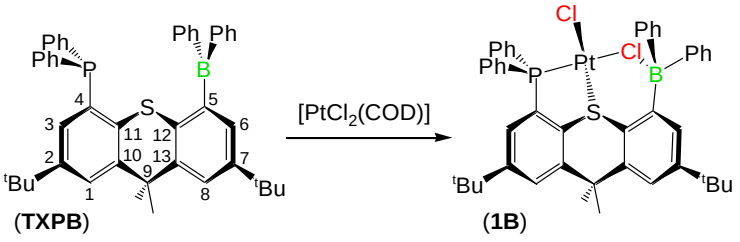

Scheme 1. Preparation of [$PtCl_2$(TXPB)] (**1B**).

X-ray quality crystals of **1B**·$2CH_2Cl_2$ were obtained by slow diffusion of hexanes into a CH_2Cl_2 solution at -30 °C (Table 1, Figure 2). Crystals of previously reported **2B** were also obtained from CH_2Cl_2/hexanes or toluene/hexanes at –30 °C; the resulting crystals, **2B**·$2CH_2Cl_2$ and solvent-free **2B**, differ in the orientation of the Pd–Cl bond with respect to the bend of the ligand backbone (Table 1, Figure 2; *vide infra*).

In **1B**·$2CH_2Cl_2$, as well as **2B** and **2B**·$2CH_2Cl_2$, the M–Cl(1) bond is considerably longer than M–Cl(2) (Table 2), which can be rationalised as a consequence of the chloro ligand–borane interaction and/or the greater trans influence of PAr_3 versus SAr_2 (*vide infra*).[11] In all chloro complexes in Table 1, the B–Cl(1) bond distances (1.98-2.15 Å) are only 0.04-0.22 Å longer than B–Cl in the chloroborate anions [CPh_3][$ClB(C_6F_5)_3$] (1.928(2) Å)[12] and [{$ClPhB(\eta^5\text{-}C_5H_4)_2$}$ZrCl_2$]$^-$ (1.937(5) Å),[13] and boron is strongly pyramidalized [Σ(C–B–C) = 337-342°]. These data, in keeping with the ^{11}B NMR chemical shifts (Table 2), are indicative of strong B–Cl interactions. Similar B–Cl distances and boron pyramidalizations have also been reported for borane functionalized [(η^3-allyl)Pd(μ-Cl){P*i*Pr_2(C_6H_4)BCy_2-*o*}] (B–Cl = 2.16 Å; Σ(C–B–C) = 349°),[14] [(Ph_3P)PdCl(μ-Cl){P*i*Pr_2(C_6H_4)BCy_2-*o*}] (B–Cl = 2.11 Å; Σ(C–B–C) = 343°),[15] [(η^2:η^2-nbd)Rh(μ-Cl){P*i*Pr_2(C_6H_4)BCy_2-*o*}] (B–Cl = 2.12 Å; Σ(C–B–C) = 343°),[15] [(*p*-cymene)RuCl(μ-Cl) (NC_5H_4(CH_2BCy_2)-*o*}] (B–Cl = 2.11 Å; Σ(C–B–C) = 347°),[16] [(κ^3-Tp)OsCl(μ-Cl){NPh(BPh_2)}] (B–Cl = 2.11 Å; Σ(C–B–C) = 347°),[17] [(η^5-Ind)TiCl(μ-Cl){$C_5H_4B(C_6F_5)_2$}] (B–Cl = 2.01 Å; Σ(C–B–C) = 342°),[18] and a B–Cl distance of 1.93 Å was calculated for the unsupported M–Cl–B bridge in [$(IMes)_2$HPt(μ-Cl){$BC_5H_4(SiMe_3)$}].[19]

In **1B**·$2CH_2Cl_2$ and **2B**·$2CH_2Cl_2$, the M–Cl–B bridge is directed towards the outside of the fold of the ligand backbone, resulting in a C(9)···S–M angle of 160-161° and an acute M–Cl–B angle of 95-96°. By contrast, in solvent-free **2B** and **3B**·hexane, the M–Cl–B bridge is directed into the fold of the ligand backbone, leading to a more acute C(9)···S–M angle of 146°, but allowing for an expanded M–

Cl–B angle of 105-108° (Table 1). Observation of both possible M–Cl–B bridge orientations in crystals of complex **2B** obtained under different conditions highlights the absence of a strong thermodynamic preference for one particular orientation in the chloro complexes. Furthermore, static structures are not preserved in solution; fluxional behaviour is observed for all of the chloro and iodo complexes in Table 1, resulting in equivalent C*Me*$_2$ groups at room temperature or slightly above.

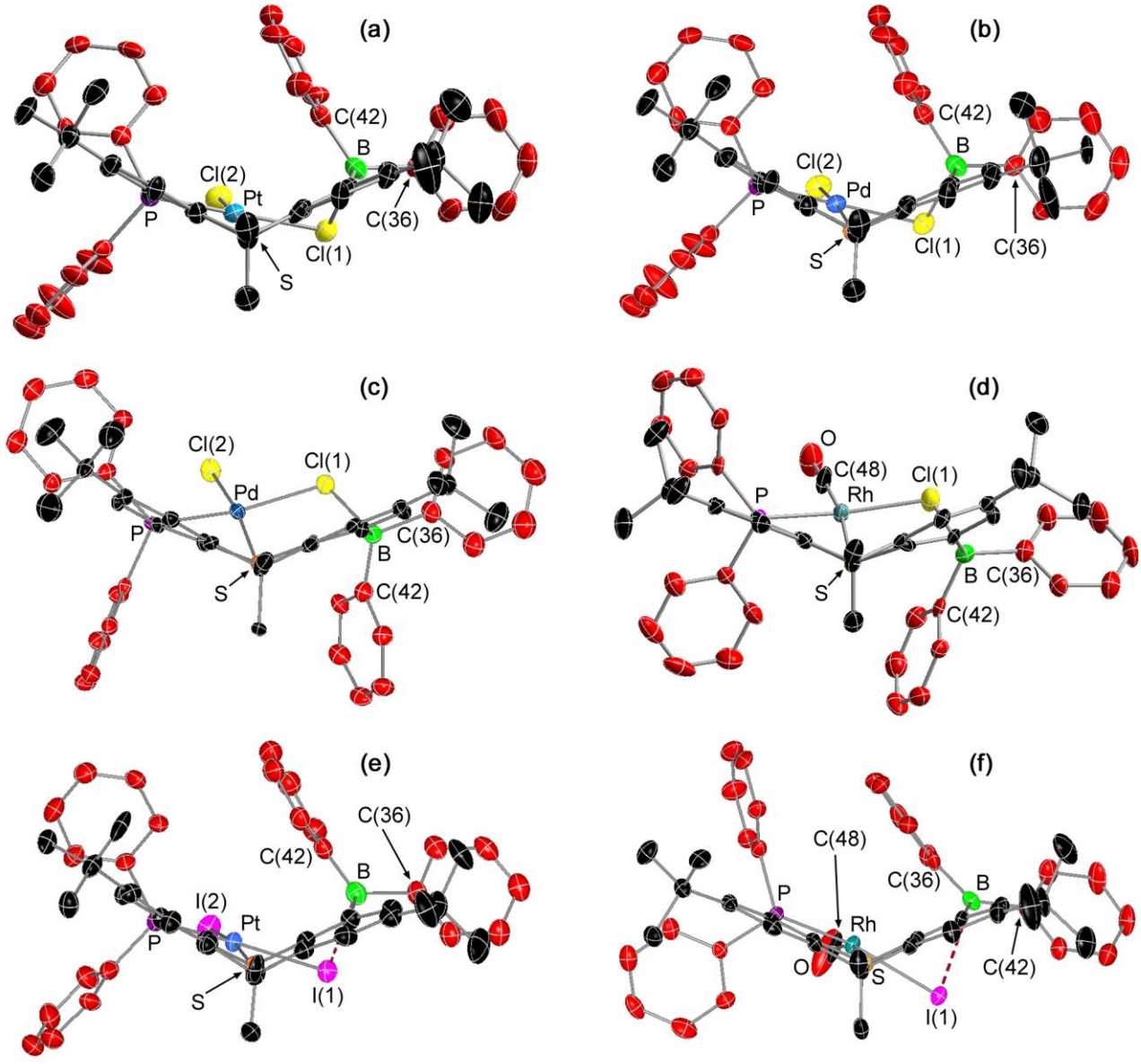

Figure 2. Solid state structures of: (a) $[PtCl_2(TXPB)]\cdot 2CH_2Cl_2$ (**1B**$\cdot 2CH_2Cl_2$), (b) $[PdCl_2(TXPB)]\cdot 2CH_2Cl_2$ (**2B**$\cdot 2CH_2Cl_2$), (c) $[PdCl_2(TXPB)]$ (**2B**), (d) previously reported [RhCl(CO)(TXPB)]·hexane (**3B**·hexane), (e) $[PtI_2(TXPB)]\cdot 1.31CH_2Cl_2$ (**4B**$\cdot 1.31CH_2Cl_2$), and (f) previously reported [RhI(CO)(TXPB)]·hexane (**5B**·hexane). Ellipsoids are at 50% probability. One CMe_3 group in **1B**$\cdot 2CH_2Cl_2$ and **2B**$\cdot 2CH_2Cl_2$ is disordered over two positions; only one orientation is shown. Hydrogen atoms and lattice solvent are omitted for clarity.

Table 1. Crystallographic data collection and refinement parameters for TXPB Complexes **1B**, **2B**, and **4B**, and TXPH complexes **2H** and **4H**.

Structure	**1B**$\cdot 2CH_2Cl_2$	**2B**	**2B**$\cdot 2CH_2Cl_2$	**4B**$\cdot 1.31CH_2Cl_2$	**2H**$\cdot 2CH_2Cl_2$	**4H**$\cdot 1.5CH_2Cl_2$
Formula	$C_{49}H_{52}BCl_6PPtS$	$C_{47}H_{48}BCl_2PPdS$	$C_{49}H_{52}BCl_6PPdS$	$C_{48.31}H_{50.62}BCl_{2.62}I_2PPtS$	$C_{37}H_{43}Cl_6PPdS$	$C_{36.5}H_{42}Cl_3I_2PPtS$
Formula wt	1122.54	863.99	1033.85	1246.93	869.84	1098.97
T (K)	173(2) K	173(2) K	173(2)	173(2)	173(2)	173(2)
Cryst. Syst.	Orthorhombic	Monoclinic	Orthorhombic	Orthorhombic	Triclinic	Triclinic
Space Group	*Pna*2(1)	*P*2(1)/*c*	*Pna*2(1)	*Pna*2(1)	*P*-1	*P*-1
a (Å)	21.373(2)	11.2575(5)	21.3801(14)	22.18(2)	12.1463(18)	12.451(2)
b (Å)	8.9593(9)	27.0326(13)	8.9678(6)	9.043(8)	12.547(2)	12.803(2)
c (Å)	25.330(3)	13.7991(7)	25.2512(17)	24.75(2)	13.883(2)	13.852(2)
α [deg]	90	90	90	90	76.402(10)	75.815(2)
β [deg]	90	97.258(3)	90	90	74.583(10)	74.648(2)
γ [deg]	90	90	90	90	81.960(10)	80.524(4)
Volume [Å^3]	4850.4(8)	4165.7(3)	4841.5(6)	4964(8)	1975.7(5)	2052.7(6)
Z	4	4	4	4	2	2
Crystal Size (mm^3)	0.24x0.18x0.01	0.17x0.12x0.02	0.32x0.28x0.12	0.25x0.13x0.03	0.30x0.30x0.15	0.06x0.05x0.03
No. of reflns collected	27401	25320	72714	34768	13584	17425
No. of indep Reflns	6568	5445	14333	9159	6736	9987
θ range for collection [deg]	2.07–26.48	1.49–22.50	1.61–30.67	1.65–26.36	1.56–24.75	2.02–28.35
Completeness to θ Max (%)	99.3	100.0	99.5	99.8	99.4	97.3
Absorption Correction	Numerical	Semi-empirical from equivalents	Numerical	Semi-empirical from equivalents	Semi-empirical from equivalents	Numerical
GOF on F^2	1.011	1.218	1.031	1.021	1.044	0.868
Final R_1 [$I > 2\sigma(I)$] (%)	4.51	9.61	4.21	6.52	8.77	6.73

Table 2. Crystallographic, spectroscopic and electrochemical data for late transition metal TXPB chloro and iodo complexes.[a]

Complex	**1B**	**2B**		**3B**	**4B**	**5B**
Metal and co-ligands	$PtCl_2$	$PdCl_2$		RhCl(CO)	PtI_2	RhI(CO)
^{31}P NMR [δ, ppm]	32.5	58.4		63.8	41.6	67.2
$^{1}J_{P,Pt}$ or $^{1}J_{P,Rh}$ [Hz]	3836	---		161	3517	167
$^{1}J_{C,Rh}$ / $^{2}J_{C,P}$ for *C*O [Hz]	---	---		77/18	---	74/14
^{11}B NMR [δ, ppm]	3	13		12	50	56
E_p vs SCE (CH_2Cl_2, 200 mVs^{-1})	E_{pc} = –1.55	E_{pc} = –0.81		E_{pa} = 0.97	E_{pc} = –1.43	E_{pa} = 0.79
ν(CO)(CH_2Cl_2/Nujol) [cm^{-1}]	---	---		2013/2010	---	2002/2004
X-ray crystal structure reference	this work	this work	this work	8	this work	8
Lattice Solvent in Crystal	2 CH_2Cl_2	2 CH_2Cl_2	none	hexane	1.31 CH_2Cl_2	hexane
M–X(1) [Å]	2.391(2)	2.396(1)	2.352(3)	2.381(2)	2.637(2)	2.664(1)
M–X(2) or M–CO [Å]	2.321(2)	2.313(1)	2.290(3)	1.82(1)	2.590(2)	1.855(7)
M–P [Å]	2.213(2)	2.226(1)	2.219(3)	2.205(2)	2.222(5)	2.224(1)
M–S [Å]	2.243(2)	2.256(1)	2.320(3)	2.379(2)	2.246(5)	2.300(1)
B–X(1) [Å]	2.14(1)	2.101(4)	1.98(1)	2.00(1)	2.75(2)	3.125(7)
M–X(1)–B [deg]	95.9(3)	94.6(1)	107.7(4)	104.6(3)	82.7(5)	74.0(1)
Σ(C–B–C) [deg]	342(2)	340(1)	337(1)	340(1)	352(2)	357(1)
S–C(12)–C(5)–B[b] [deg]	20(2)	19.6(4)	–5(2)	–13(1)	26(3)	17(1)
C(9)···S–M (deg)	160	161	146	146	163	165
M–(PCCSplane)[c] [Å]	0.54	0.57	1.05	1.02	0.45	0.14
B–(CCCplane)[d] [Å]	0.46	0.42	0.45	0.43	0.26	0.16
Ligand bend[e] [deg]	51	51	47	43	53	53

(a) In the X-ray crystal structures of **1B**-**5B**, atoms C(1)-C(13) of the xanthene ligand backbone are numbered as shown in Scheme 1. (b) positive S–C(12)–C(5)–B torsion angles indicate that boron is oriented up into the fold of the thioxanthene backbone. (c) PCCSplane = P–C4–C11–S. (d) CCC plane = C5–C36–C42. (e) Ligand bend = the angle between the two aromatic rings in the thioxanthene backbone of the ligand [i.e. the angle between the C(1)/C(2)/C(3)/C(4)/C(10)/C(11) and C(5)/C(6)/C(7)/C(8)/C(12)/C(13) planes].

Reaction of [PtI_2(COD)] with TXPB gave bright yellow [PtI_2(TXPB)] (**4B**) in 73 % isolated yield (Scheme 2). The ^{11}B NMR signal at 50 ppm is indicative of a weaker PtX···B interaction than in related chloro TXPB complexes (*cf.* 69 ppm for free TXPB ligand[7] and 3-13 ppm for **1B**-**3B**). An analogous situation was observed for previously prepared [RhI(CO)(TXPB)] (**5B**; ^{11}B NMR δ 56 ppm).[8]

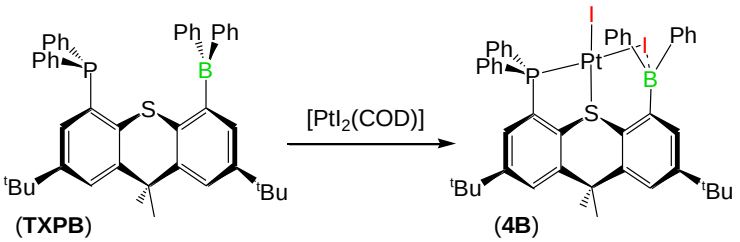

Scheme 2. Preparation of [PtI_2(TXPB)] (**4B**).

X-ray quality crystals of **4B**·1.31CH_2Cl_2 were grown from CH_2Cl_2/hexanes at –30 °C. The solid state structure of **4B** (Table 1, Figure 2) revealed approximate square planarity at platinum [P–Pt–I(1) = 175.0(1)° and S–Pt–I(2) = 171.8(1)°] and an M–X–BR_3 bridging interaction directed towards the outside of the fold of the ligand backbone; an analogous arrangement was observed in the platinum chloro analogue **1B**. The B···I distance[20] in **4B** is 2.75(2) Å. Structurally characterized iodoborates (BR_3I^-) are not available for comparison, but this distance is approximately 0.5 Å longer than the B–I bond in crystallographically characterised iodoboranes (c.f. 2.15-2.17 Å in 1,3,5-triiodo-1,3,5-triborocyclohexane,[21] and 2.22-2.25 Å in Me_3PBI_3).[22] The boron atom in **4B** is also pyramidalized to a much lesser extent [Σ(C–B–C) = 353(3)°] than in **1B**, **2B** or **3B** [Σ(C–B–C) = 337–342°]. For comparison, the B–I distance in rhodium iodo complex **5B** is 3.125(7) Å and the sum of the C–B–C angles is 357(1)°.[8] The Pt–I(1) bond (trans to PAr_3; 2.637(2) Å) in **4B** is significantly longer than Pt–I(2) (trans to SAr_2; 2.590(2) Å), presumably as a consequence of the iodo ligand–borane interaction and/or the greater trans influence of PAr_3 versus SAr_2;[11] the latter effect is expected to dominate given the long B–I distance in **4B**.

Complexes of a borane-free analogue of TXPB: To probe in more detail the factors responsible for differences in the M–X(1) and M–X(2) bond lengths in **1B**, **2B**, and **4B**, and the nature of M–X–BR_3 interactions, complexes of a borane free analogue of TXPB, 2,7-di-*tert*-butyl-4-diphenylphosphino-9,9-dimethylthioxanthene (**TXPH**), were prepared.

The TXPH ligand was accessed by lithiation of 2,7-di-*tert*-butyl-4-bromo-5-diphenylphosphino-9,9-dimethylthioxanthene (**TXPBr**)[7] followed by quenching with deoxygenated MeOH. Reaction of [$PtCl_2$(COD)], [$PdCl_2$(COD)], 0.5 [{RhCl$(CO)_2$}$_2$] and [PtI_2(COD)] with TXPH then provided [$PtCl_2$(TXPH)] (**1H**), [$PdCl_2$(TXPH)] (**2H**), [RhCl(CO)(TXPH)] (**3H**) and [PtI_2(TXPH)] (**4H**), respectively (Scheme 3). As in complex **3B**, the CO ligand in **3H** is *cis* to the phosphine donor, based on

a $^2J_{C,P}$ coupling of 16 Hz.[23] Sharp CO stretches at 2010 cm^{-1} and 2001 cm^{-1} were observed for **3B** and **3H** respectively in Nujol, indicative of decreased electron density at the metal centre in **3B**. However, a very broad carbonyl stretch at 2013 cm^{-1} was observed for both complexes in CH_2Cl_2.

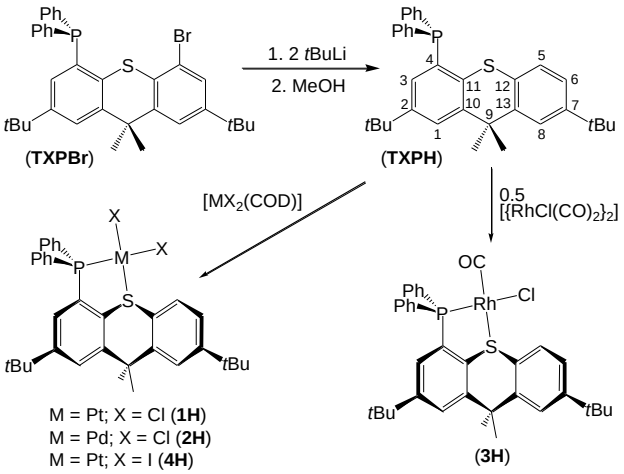

Scheme 3. Preparation and complexation of the TXPH ligand.

X-Ray quality crystals of **2H**·2CH_2Cl_2 and **4H**·1.5CH_2Cl_2 were grown by slow diffusion of hexanes into CH_2Cl_2 solutions of each complex at –30 ºC (Table 1, Figure 3). Both complexes are square planar with M–P, M–S, M–X(1) and M–X(2) bond distances (Table 3) very close to those in the TXPB analogues (Table 2). These data highlight that in complexes **2B** and **4B** (and by extrapolation, **1B**), the greater *trans*-influence of PAr_3 versus SAr_2 donors[11] is the major factor responsible for elongation of the M–X(1) bond relative to M–X(2). In both **2H**·2CH_2Cl_2 and **4H**·1.5CH_2Cl_2, C9···S–M angles of 158° were observed, and the M–X(1) bond is directed towards the outside of the fold of the ligand backbone, leading to C9···S–M angles in the 157-165° range. This M–X(1) bond orientation is analogous to that in **1B**·2CH_2Cl_2, **2B**·2CH_2Cl_2, **4B**·1.31CH_2Cl_2, and **5B**·hexane, but not **2B** or **3B**·hexane.

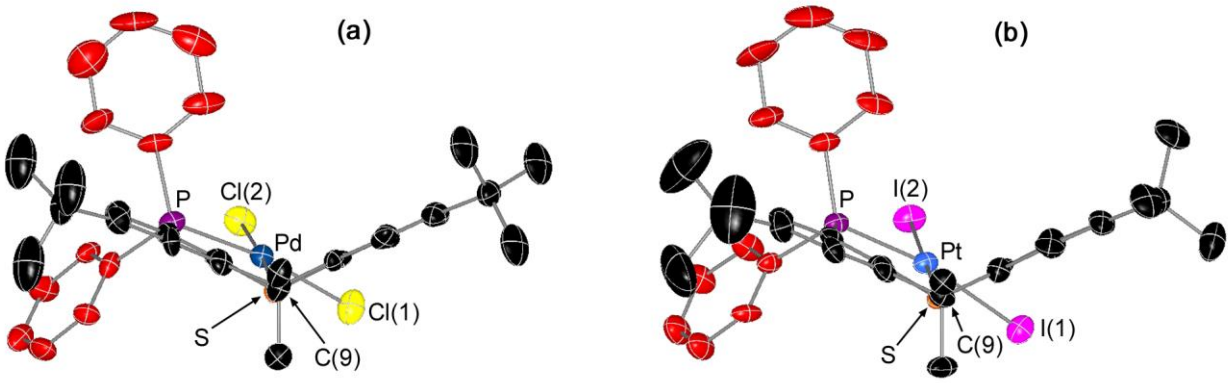

Figure 3. Solid state structures for: (a) $[PdCl_2(TXPH)]\cdot 2CH_2Cl_2$ (**2H**$\cdot 2CH_2Cl_2$) and (b) $[PtI_2(TXPB)]\cdot 1.5CH_2Cl_2$ (**4H**$\cdot 1.5CH_2Cl_2$) with ellipsoids at 50% probability. Both CMe_3 groups in **2H**$\cdot 2CH_2Cl_2$ and one CMe_3 group in **2B**$\cdot 2CH_2Cl_2$ are disordered over two positions; only one orientation is shown. Hydrogen atoms and lattice solvent are omitted for clarity.

Table 3. Spectroscopic, Crystallographic and Electrochemical Data for TXPH complexes.

Complex	**1H**	**2H**	**3H**	**4H**
Metal and co-ligands	$PtCl_2$	$PdCl_2$	RhCl(CO)	PtI_2
^{31}P NMR [δ, ppm]	38.6	61.4	69.5	43.6
$^1J_{C,Rh}$ / $^2J_{C,P}$ for *C*O [Hz]	---	---	78/16	---
$^1J_{P,Pt}$ or $^1J_{P,Rh}$ [Hz]	3458	---	148	3251
E_p vs SCE (CH_2Cl_2, 200 mVs^{-1})	E_{pc} = –1.63	E_{pc} = –1.11	ill defined	E_{pc} = –1.45
ν(CO)(CH_2Cl_2/Nujol) [cm^{-1}]	---	---	2013/2001	---
Lattice solvent in crystal	---	2 CH_2Cl_2	---	1.5 CH_2Cl_2
M–X(1) [Å]	---	2.369(3)	---	2.658(1)
M–X(2) or M–CO [Å]	---	2.308(3)	---	2.607(1)
M–P [Å]	---	2.216(3)	---	2.232(3)
M–S [Å]	---	2.260(3)	---	2.258(3)
C(9)···S–M (deg)	---	158	---	158
Ligand bend[a] (deg)	---	48	---	49

(a) Ligand bend = the angle between the two aromatic rings in the thioxanthene backbone of the ligand [i.e. the angle between the C(1)/C(2)/C(3)/C(4)/C(10)/C(11) and C(5)/C(6)/C(7)/C(8)/C(12)/C(13) planes]. In the X-ray crystal structures of **2H** and **4H**, atoms C(1)-C(13) of the xanthene ligand backbone are numbered as shown in Scheme 3.

Electrochemistry of chloro and iodo complexes: All TXPB complexes and their TXPH analogues were investigated by cyclic voltammetry (CV) in CH_2Cl_2 (platinum disk electrode, $[NBu_4][PF_6]$ base electrolyte, $FeCp^*_2$ calibrant; Tables 2 and 3). Palladium and platinum complexes exhibited an irreversible reduction peak while rhodium complexes **3B** and **5B** gave rise to an irreversible oxidation

peak. At a scan rate of 200 mV s^{-1}, the E_{pc} values for **4B** and **4H** are equal within error. By contrast, the E_{pc} values for the Pd and Pt chloro TXPB complexes are less negative, by 80-300 mV, than those for TXPH analogues, suggesting decreased electron density at the metal centre in chloro TXPB complexes. However, these differences should be viewed with some caution given the sensitivity of irreversible peak potentials to parameters such as uncompensated resistance, diffusion coefficients and test complex concentration ($E_{1/2}$ values are insensitive to these parameters).[24] More reversible redox behaviour was not observed in a CV of **2H** in CH_2Cl_2 at –78 °C using $[NBu_4][B(C_6F_5)_4]$ as the base electrolyte.

DFT Calculations:

To further investigate the strength and consequences of halide ligand–borane coordination, DFT calculations (ADF, all-electron, TZ2P, ZORA, VWN, PW91) were carried out on **1B-5B** (for complex **2B**, the geometry in **2B**·$2CH_2Cl_2$ was used as the starting point for geometry optimization), **1H-4H**, and [RhI(CO)(TXPH)] (**5H**). The geometry optimized structures for crystallographically characterized **1B-5B, 2H** and **4H** match closely with experimental values (Table 4). For example, calculated M–P, M–S, M–X bond lengths lie within 0.05 Å (2 %) of the experimental values, and the calculations satisfactorily reproduced the bond angles at the metal (< 1.5 % deviation for TXPB complexes and < 3.5 % deviation for TXPH complexes). M–X–B bond angles were also reproduced to within 6 % of crystallographic values, and calculated B–X bond distances in the TXPB complexes differed from crystallographically determined values by 1.5-3 % in **1B-3B** and **5B** and 5 % in **4B**. The larger difference between calculated and crystallographic bond lengths in **4B** may be a consequence of a particularly shallow potential energy surface asociated with changes in the B–X bond length in iodo complexes.

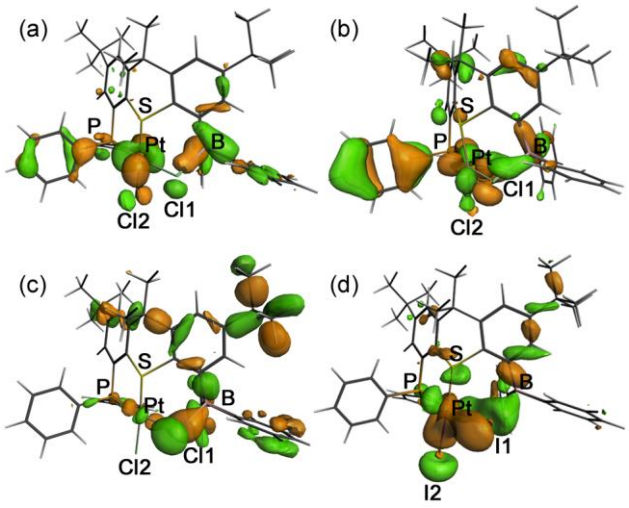

Figure 4. Slater-type Molecular orbitals involved in B–X(1) bonding in chloro complex **1B** and iodo complex **4B**: (a) HOMO–13 in **1B**, (b) HOMO–17 in **1B**, (b) HOMO–28 in **1B**, (b) HOMO–21 in **4B**. Isosurfaces are set to 0.03.

At least one molecular orbital involved in B–X(1) bonding was observed for all TXPB complexes (Figure 4), and selected Mayer bond orders[25] and Hirshfeld charges[26] are listed in Table 5. The B–X(1) Mayer bond orders are 0.626, 0.654, 0.639, 0.585 and 0.337 in **1B**, **2B**, **3B**, **4B** and **5B** (the B–I(1) Mayer bond order is 0.509 for the TZ2P geometry optimized structure of **4B** with the B–X(1) bond constrained to the crystallographically determined bond distance). These data are indicative of greater covalency in B–Cl bonds relative to B–I bonds, despite the higher electronegativity of chlorine. However, they do not provide direct insight into the strength of B–Cl versus B–I bonding.

Now comparing TXPB complexes with their TXPH analogues, the differences in M–P, M–S and M–X(2) Mayer bond orders are never more than 4 %. By contrast, the M–X(1) Mayer bond orders for **1B**-**5B** are 19, 27, 20, 10 and 8 % lower than the corresponding bond orders for **1H**-**5H**, indicating that the M–X(1) bonds in all five TXPB complexes are weakened as a result of borane complexation; to a greater extent in chloro complexes **1B**-**3B**. Calculated M–X(1) bond distances are also elongated (by

0.049, 0.070 and 0.030 Å) in chloro TXPB complexes **1B**-**3B**, relative to TXPH analogues. By contrast, the M–X(1) bonds in **4B** and **5B** lie within 0.01 Å of the M–X(1) distances in their TXPH analogues.

Borane coordination in TXPB complexes also results in less negative Hirshfeld charges on X(1), relative to TXPH complexes; Hirshfeld charges on X(1) lie in the –0.01 to –0.14 range for **1B**-**5B**, compared with –0.27 to –0.37 in **1H**-**5H**. These changes as a result of boron–halide coordination are accompanied by a slight reduction in the positive charge on boron; Hirshfeld charges on boron are 0.02-0.04 in **1B**-**4B** and 0.08 in **5B**, compared with 0.12 in the free TXPB ligand (for comparison, the Hirshfeld charges on boron and iodine are 0.01 and –0.25 in the $[TXPB–I]^-$ anion calculated at the same level of theory; B–I = 2.456 Å; Σ (C–B–C) = 339.1°; B-I Mayer bond order = 0.793).

Table 4. Calculated bond lengths (Å) and angles (°) for complexes **1B**-**5B** and **1H**-**5H** [Y = X(2) or CO]. Where available, crystallographic values[a] are shown in square brackets.[27]

Compound	**1B**	**1H**	**2B**	**2H**	**3B**	**3H**	**4B**	**4H**	**5B**	**5H**
MXY	$PtCl_2$	$PtCl_2$	$PdCl_2$	$PdCl_2$	RhCl(CO)	RhCl(CO)	PtI_2	PtI_2	RhI(CO)	RhI(CO)
M–P	2.222 [2.213(2)]	2.224	2.233 [2.226(1)]	2.239 [2.216(3)]	2.225 [2.205(2)]	2.229	2.243 [2.222(5)]	2.243 [2.232(3)]	2.241 [2.224(1)]	2.236
M–S	2.248 [2.243(2)]	2.257	2.258 [2.256(1)]	2.286 [2.260(3)]	2.394 [2.379(2)]	2.379	2.276 [2.246(5)]	2.279 [2.258(3)]	2.320 [2.300(1)]	2.383
M–X(1)	2.414 [2.391(2)]	2.365	2.428 [2.396(1)]	2.358 [2.369(3)]	2.399 [2.381(2)]	2.369	2.689 [2.637(2)]	2.690 [2.658(1)]	2.699 [2.664(1)]	2.690
M–Y	2.324 [2.321(2)]	2.323	2.319 [2.313(1)]	2.320 [2.308(3)]	1.841 [1.82(1)]	1.841	2.643 [2.590(2)]	2.640 [2.607(1)]	1.845 [1.855(7)]	1.839
B–X(1)	2.107 [2.14(1)]	---	2.065 [2.101(4)]	---	2.040 [2.00(1)]	---	2.614 [2.75(2)]	---	3.043 [3.125(7)]	---
P–M–X(1)	173.9 [174.8(1)]	177.5	171.9 [173.35(3)]	176.8 [171.1(1)]	170.6 [172.6(1)]	175.9	174.4 [175.0(1)	173.3 [169.3(1)]	170.5 [169.58(4)]	173.2
S–M–Y	172.5 [173.4(1)]	178.1	173.2 [171.80(3)]	175.6 [175.7(1)]	169.2 [171.3(3)]	172.5	172.2 [171.8(1)]	179.8 [178.3(1)]	166.1 [163.8(2)]	174.1
M–X(1)–B	98.3 [95.9(3)]	---	98.6 [94.6(1)]	---	105.0 [104.6(3)]	---	87.7 [82.7(5)]	---	78.0 [74.0(1)]	---
Σ(C–B–C)	340.8 [342(2)]	---	338.9 [340(1)]	---	339.0 [340(1)]	---	346.6 [352(2)]	---	353.9 [357(1)]	---

(a) For complex **2B**, crystallographic values are from **2B**·$2CH_2Cl_2$.

Table 5. Mayer bond orders (MBO) Hirshfeld charges, and Energy Decomposition Analysis data for complexes **1B-5B** and **1H-5H**. Hirshfeld charges for MXY and L are from fragment analysis [X = X(1), Y = X(2) or CO, L = TXPB or TXPH].[27]

Compound	**1B**	**1H**	**2B**	**2H**	**3B**	**3H**	**4B**	**4H**	**5B**	**5H**
MXY	$PtCl_2$	$PtCl_2$	$PdCl_2$	$PdCl_2$	RhCl(CO)	RhCl(CO)	PtI_2	PtI_2	RhI(CO)	RhI(CO)
M–P MBO	1.211	1.212	1.098	1.068	1.1774	1.152	1.170	1.165	1.1609	1.1293
M–S MBO	1.040	1.023	0.922	0.884	0.7447	0.7695	0.983	0.980	0.8590	0.7660
M–X(1) MBO	0.645	0.766	0.569	0.723	0.6047	0.7234	0.729	0.804	0.6889	0.7466
Δ[M–X(1)][a]	*19 %*		*27 %*		*20 %*		*10 %*		*8 %*	
M–Y MBO	0.849	0.839	0.794	0.777	1.3126	1.289	0.904	0.905	1.2875	1.2611
B–X(1) MBO	0.626	---	0.654	---	0.6387	---	0.5850	---	0.3368	---
M Hirshfeld	0.1330	0.103	0.3238	0.2960	0.0410	0.0080	0.0668	0.0394	0.0180	–0.0221
X(1) Hirshfeld	–0.0497	–0.3103	–0.0825	–0.3671	–0.0319	–0.3204	–0.0114	–0.2660	–0.1448	–0.2710
Δ[X(1) Hirsh][b]	*0.2606*		*0.2846*		*0.2885*		*0.2546*		*0.1262*	
X(2) Hirshfeld	–0.2529	–0.2629	–0.3118	–0.3099	---	---	–0.1931	–0.2027	---	---
B Hirshfeld	0.0347	---	0.0230	---	0.0231	---	0.0430	---	0.0847	---
MXY Hirshfeld	–0.2076	–0.3537	–0.2107	–0.3537	–0.0449	–0.1652	–0.2412	–0.3949	–0.1231	–0.1832
L Hirshfeld	0.2077	0.3539	0.2112	0.3539	0.0449	0.1656	0.2418	0.3951	0.1238	0.1838
Δ[L Hirsh][c]	*–0.1462*		*–0.1427*		*–0.1207*		*–0.1533*		*–0.0600*	
ΔE_{int}	–573	–493	–491	–383	–477	–367	–455	–425	–368	–348
Δ(ΔE_{int})	*–80*		*–108*		*–110*		*-30*		*–19*	
ΔE_{orb}	–1030	–756	–905	–583	–810	–516	–880	–718	–605	–503
Δ(ΔE_{orb})	*–274*		*–322*		*–294*		*–163*		*–102*	
ΔE_{elec}	–1344	–1152	–1102	–869	–982	–784	–1258	–1157	-877	–792
Δ(ΔE_{elec})	*–192*		*–233*		*–198*		*–101*		*–85*	
ΔE_{Pauli}	1801	1414	1516	1068	1315	933	1684	1450	1115	947
Δ(ΔE_{Pauli})	*387*		*448*		*382*		*234*		*168*	

(a) Δ[M–X(1)] = [(M–X(1) distance in TXPH complex / M–X(1) distance in TXPB analogue) * 100] – 100.
(b) Δ[X(1) Hirsh] = 'X(1) Hirshfeld' for TXPB complex – 'X(1) Hirshfeld' for TXPB analogue.
(c) Δ[L Hirsh] = 'L Hirshfeld' for TXPB complex – 'L Hirshfeld' for TXPH analogue.
(d) ΔE_x in kJ mol^{-1}. ΔE_{int} = total interaction energy; ΔE_{orb} = orbital mixing energy; ΔE_{elec} = electrostatic interaction energy; ΔE_{Pauli} = Pauli repulsion energy; $\Delta(\Delta E_x) = \Delta E_x$ (TXPB_complex)– ΔE_x(TXPH_analogue).

All TXPB and TXPH complexes were further investigated through a fragment approach that considered the interaction of an uncharged MX_2 (M = Pt or Pd) or RhX(CO) fragment with a neutral TXPB or TXPH ligand (fragments were generated from the TZ2P geometry optimized structures of each complex). For each TXPB complex and TXPH analogue, the Hirshfeld charge on the TXPB fragment is less positive than the Hirshfeld charge on the TXPH fragment by 0.06 to 0.15 electrons, consistent with donation of electron density from X(1) to boron. Regions in which electron density is depleted or increased upon combination of each MX_2 or MX(CO) fragment with TXPB or TXPH are illustrated in the SCF deformation density (SCF electron density for the molecule minus the sum of the SCF electron density for the two fragments) isosurfaces in Figure 5. These isosurfaces clearly show electron donation from the halide to the borane in both the chloro and iodo TXPB complexes.

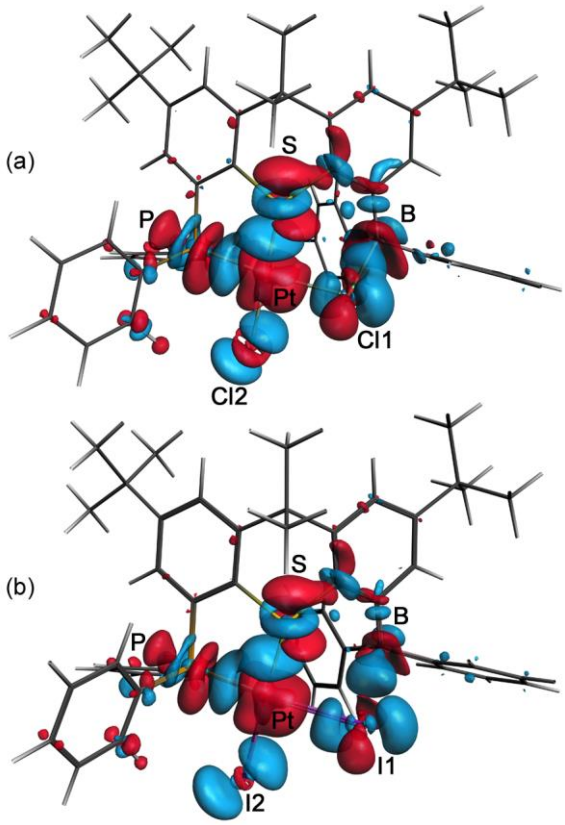

Figure 5. SCF deformation density isosurfaces from fragment analysis of: (a) chloro complex **1B** and (b) iodo complex **4B**. Blue represents increased electron density and red represents depleted electron density, relative to the constituent MX_2 and TXPB fragments (isosurfaces are set to 0.003).

Particularly valuable insight into the bonding situation in TXPB complexes was gained through Energy Decomposition Analysis of **1B-5B** and **1H-5H** (Table 5, Figure 6), which partitions the total interaction energy (ΔE_{int}) between two prepared fragments into three major components: (1) orbital mixing (ΔE_{orb}), which includes electron pair bonding, charge-transfer, donor-acceptor interactions, and intrafragment polarization, (2) the electrostatic interaction energy (ΔE_{elec}), which is typically dominated by nucleus-electron attractions, and (3) Pauli repulsion (ΔE_{Pauli}) which arises from destabilizing interfragment interactions between electrons with the same spin.

The orbital mixing contribution is substantially more negative in TXPB complexes relative to their TXPH analogues; by 274 to 322 kJ mol^{-1} in **1B-3B**, 163 kJ mol^{-1} in **4B**, and 102 kJ mol^{-1} in **5B**. These data support the presence of a strong covalent contribution to B–Cl(1) bonding, and a weaker but still significant covalent contribution to B–I(1) bonding. In TXPB complexes, the electrostatic contribution to bonding is also more negative than that in TXPH analogues, and this difference is markedly more pronounced in chloro complexes than iodo complexes; ΔE_{elec}(TXPB_complex)–ΔE_{elec}(TXPH_complex) is –192 to –233 kJ mol^{-1} in **1B-3B**, compared with –101 and –85 kJ mol^{-1} in **4B** and **5B**. These data are commensurate with the greater electronegativity of chlorine versus iodine, and the shorter B–X distances in chloro versus iodo complexes. In contrast to the orbital mixing and electrostatic terms, the Pauli repulsion term is more positive in TXPB complexes relative to TXPH analogues; by approx. 400 kJ mol^{-1} in **1B-3B** and approx. 200 kJ mol^{-1} in **4B** and **5B**. The larger Pauli repulsion term in chloro versus iodo TXPB complexes presumably arises due to closer approach of the borane and the chloro ligand.

Overall, the total interaction energy (ΔE_{int}) for combination of an MX_2 or MX(CO) fragment with a TXPB or TXPH fragment is more positive in TXPB complexes than in TXPH analogues, and this difference is more pronounced in chloro complexes than iodo complexes; ΔE_{int}(TXPB_complex)–ΔE_{int}(TXPH_complex) is –80 to –110 kJ mol^{-1} in **1B-3B**, compared with –30 and –19 kJ mol^{-1} in **4B** and **5B**. In chloro TXPB complexes, the larger contribution (relative to iodo TXPB complexes) from B–X bonding to the total interaction energy arises from significantly more negative orbital mixing and electrostatic terms which are partially offset by a larger Pauli repulsion term. The presence of a significantly stronger B–X interaction in chloro complexes relative to iodo complexes is commensurate with the experimentally determined ^{11}B NMR chemical shifts, B–X distances, and C–B–C angles. The relative weakness of the B–I interactions in **4B** and **5B** is consistent with the poor match between a fairly hard borane Lewis acid and a soft iodide anion. Indeed, $[NBu_4][BI_4]$ is reported to be extremely labile,[28] $[NEt_4][BI_4]$ is proposed to ionize to $[NEt_4]^+$, $[BI_2(NCMe)_2]^+$ and I^- (2 equiv.) upon dissolution in

acetonitrile,[29] in the reaction of BPh_3 with $[NEt_4]I$ in CH_2Cl_2, the equilibrium lies towards the reactants rather than the iodoborate salt, and $[Co(C_5H_4B^iPr_2I)(C_5H_4B^iPr_2)]$ is substantially dissociated to $[Co(C_5H_4B^iPr_2)_2]I$ in CH_2Cl_2.[30] However, BI_4^- salts of $[C_7H_7]^+$, $[CPh_3]^+$,[31] $[C_5Me_5BI]^+$,[32] and $[\{Si(Si^tBu_3)\}_4I]^+$ cations[33] have been reported, as has $[C_7H_7][PhBI_3]$.[34]

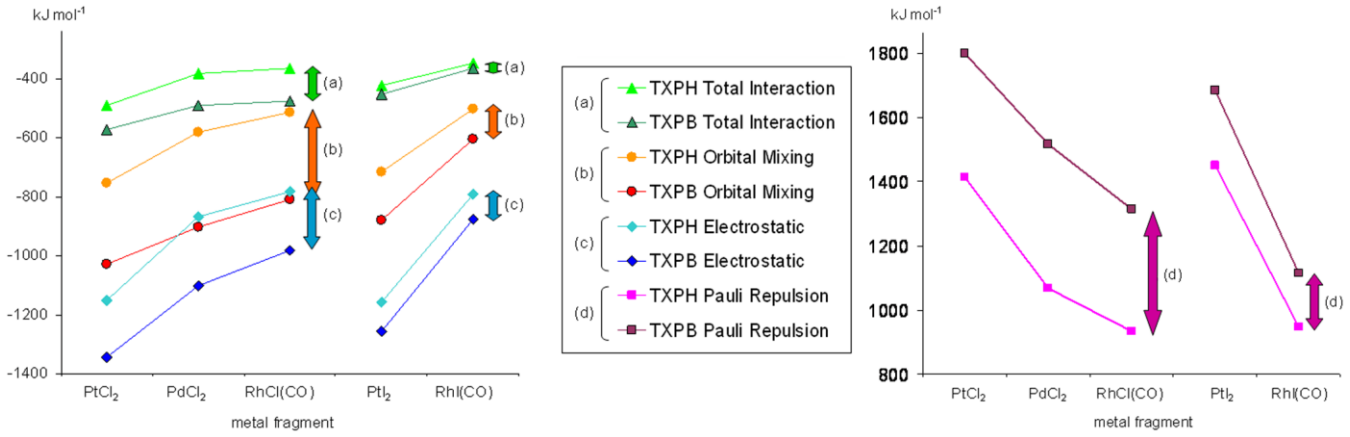

Figure 6. Graphs of (a) ΔE_{int}, (b) ΔE_{orb}, (c) ΔE_{elec}, and (d) ΔE_{Pauli} from Energy Decomposition Analysis of complexes **1B**–**5B** and **1H**–**5H** using MX_2, MX(CO), TXPB and TXPH fragments in conformations corresponding to those in each complex. Double headed arrows are provided for graphical comparison of the magnitude of ΔE_x(TXPB_complex)–ΔE_x(TXPH_complex) (x = int, orb, elec or Pauli) between chloro and iodo complexes.

Conclusions:

Chloro TXPB complexes **1B**, **2B** and **3B** exhibit strong M–Cl(1)–BR_3 bridging interactions, resulting in B–Cl(1) distances that are only 0.04-0.22 Å longer than those reported for chloroborate complexes, significant pyramidalization at boron, and approx. 60 ppm shifts in the ^{11}B NMR signal to low frequency of free TXPB. By contrast, TXPB iodo complexes **4B** and **5B** display B–I(1) distances that are roughly 0.5 Å longer than those reported for iodoboranes, only slight pyramidalization at boron, and ^{11}B NMR signals that are shifted 10-20 ppm to low frequency of free TXPB. Structural, spectroscopic and/or

computational comparison of TXPB complexes **1B-5B** with TXPH complexes **1H-5H** allowed for more detailed analysis of M–X(1)–BR_3 interactions in TXPB complexes. Crystallographically and computationally determined M–X(1) and M–X(2) bond lengths revealed that the differing trans-influence of PAr_3 and SAr_2 donors plays a major role in the elongation of M–X(1) bonds relative to M–X(2) bonds. However, in all TXPB complexes, borane-coordination does result in reduced M–X(1) Mayer bond orders and smaller Hirshfeld charges on X(1) relative to TXPH analogues. Energy decomposition analysis using MX_2 or MX(CO) and TXPB or TXPH fragments revealed a larger contribution from B–X bonding to the total interaction energy in chloro TXPB complexes, relative to iodo TXPB complexes; ΔE_{int}(TXPB_complex)–ΔE_{int}(TXPH_complex) is –80 to –110 kJ mol^{-1} in **1B-3B** versus –30 and –19 kJ mol^{-1} in **4B** and **5B**. The larger contribution in chloro complexes arises from significantly more negative orbital mixing and electrostatic terms which are partially offset by a larger Pauli repulsion term. The presence of a significantly stronger B–X interaction in chloro complexes relative to iodo complexes is consistent with the trends in B–X Mayer bond order, ^{11}B NMR chemical shift, irreversible peak potentials from cyclic voltammetry, B–X distance, and C–B–C angle.

Experimental Section

General Details. An argon-filled MBraun UNIlab glove box equipped with a –30 °C freezer was employed for the manipulation and storage of the TXPB ligand and its complexes, and reactions were performed on a double manifold high vacuum line using standard techniques.[35] A Fisher Scientific Ultrasonic FS-30 bath was used to sonicate reaction mixtures where indicated. Residual oxygen and moisture was removed from the argon stream by passage through an Oxisorb-W scrubber from Matheson Gas Products.

Anhydrous CH_2Cl_2 was purchased from Aldrich. Hexanes and toluene were initially dried and distilled at atmospheric pressure from CaH_2 and Na, respectively. Unless otherwise noted, all proteo solvents were stored over an appropriate drying agent (toluene, benzene = Na/Ph_2CO; hexanes =

Na/Ph_2CO/tetraglyme; CH_2Cl_2 = CaH_2) and introduced to reactions via vacuum transfer with condensation at –78°C. The deuterated solvents CD_2Cl_2 and C_6D_5Br (ACP Chemicals) were dried over CaH_2. [$PdCl_2$(COD)], [$PtCl_2$(COD)] and [PtI_2(COD)] were purchased from Strem Chemicals. [{RhCl(CO)$_2$}$_2$] and ^{t}BuLi (1.7 M in pentane) were purchased from Sigma-Aldrich. Prior to use, ^{t}BuLi solutions were titrated with *N*-benzylbenzamide (Aldrich) at –45 °C.[36] The compounds TXPBr and TXPB were prepared as previously described.[7]

NMR spectroscopy (^{1}H, ^{13}C{^{1}H}, DEPT-135, DEPTq, COSY, HSQC, HMBC) was performed on Bruker DRX-500 and AV-600 spectrometers. All ^{1}H NMR and ^{13}C NMR spectra were referenced relative to $SiMe_4$ through a resonance of the employed deuterated solvent or proteo impurity of the solvent; CD_2Cl_2 (5.32 ppm), C_6D_5Br (δ 7.30, 7.02, 6.94 ppm) for ^{1}H NMR, and CD_2Cl_2 (54.0 ppm), C_6D_5Br (δ130.9, 129.3, 126.1, 122.3 ppm) for ^{13}C NMR. Herein, numbered proton and carbon atoms refer to the positions of the xanthene backbone in the TXPB or TXPH ligands (see Schemes 1 and 3).

Combustion elemental analyses were performed on a Thermo EA1112 CHNS/O analyzer and IR spectra were recorded on a Bio-Rad FTS-40 FTIR instrument. Cyclic voltammetry (CV) studies were carried out using a PAR (Princeton Applied Research) model 283 potentiostat (using PAR PowerCV software) in conjunction with a three-electrode cell under an argon atmosphere. The auxiliary electrode was a platinum wire, the pseudo-reference electrode a silver wire, and the working electrode a platinum disc (1.6 mm diameter, Bioanalytical Systems). Solutions were 1 x 10^{-3} M in test compound and 0.1 M in [N^nBu_4][PF_6] as the supporting electrolyte in CH_2Cl_2. In all experiments, potentials were calibrated by addition of [FeCp*$_2$]; the $E_{1/2}$ value for [FeCp*$_2$]$^{0/+1}$ is –0.07 V versus the SCE.[37]

X-ray crystallographic analyses were performed on suitable crystals coated in Paratone oil and mounted on either: (a) a P4 diffractometer with a Bruker Mo rotating-anode generator and a SMART1K CCD area detector, or (b) a SMART APEX II diffractometer with a 3 kW Sealed tube Mo generator, both in the McMaster Analytical X-Ray (MAX) Diffraction Facility. In all cases, non-hydrogen atoms were refined anisotropically and hydrogen atoms were generated in ideal positions and then updated with

each cycle of refinement. The following groups were rotationally or positionally disordered over two positions: (a) one of the *tert*-butyl substituents in **1B**·2CH_2Cl_2, (b) both molecules of CH_2Cl_2 in **1B**·2CH_2Cl_2, (c) one of the *tert*-butyl substituents in **2B**·2CH_2Cl_2, (d) both molecules of CH_2Cl_2 in **2B**·2CH_2Cl_2, (e) both of the *tert*-butyl substituents in **2H**·2CH_2Cl_2, (f) one of the *tert*-butyl substituents in **4H**·1.5CH_2Cl_2, and (g) one molecule of CH_2Cl_2 in **4H**·1.5CH_2Cl_2; the other half molecule of CH_2Cl_2 was SQUEEZED from this lattice due to unresolveable disorder.[38]

In all cases, disorder was modeled allowing occupancy and positional parameters to refine freely. All *tert*-butyl methyl groups in cases (a), (c), (e) and (f) above were restrained to have equivalent thermal parameters, and were refined anisotropically. The quaternary carbon–methyl carbon bond distances within the disordered *tert*-butyl substituents in **1B**·2CH_2Cl_2, **2B**·2CH_2Cl_2, **2H**·2CH_2Cl_2, and **4H**·1.5CH_2Cl_2 were restrained to approximately 1.54 Å. In addition, the C_{methyl}–C–C_{methyl} bond angles in the disordered *tert*-butyl substituent in **1B**·2CH_2Cl_2 were restrained to approximately 109.5°. For cases (a), (c), and (f), the disorder found within each of the modelled *tert*-butyl substituents was equal to 0.59(1), 0.637(5), and 0.41(1), respectively. For case (e), the disorder found within the *tert*-butyl substituents was 0.46(3) (C16–C19) and 0.14(1) (C20–C23). The carbon–chlorine bond distances in molecules of CH_2Cl_2 found in **1B**·2CH_2Cl_2, **2B**·2CH_2Cl_2, **4B**·1.31CH_2Cl_2 and **4H**·1.5CH_2Cl_2 were restrained to approximately 1.77 Å. For cases (b), (d) and (g), CH_2Cl_2 carbon and chlorine atoms were restrained to have equivalent thermal parameters, respectively. For case (b), CH_2Cl_2 carbon and chlorine atoms were refined using the ISOR command; unrestrained anisotropic refinement of the CH_2Cl_2 molecules resulted in unstable refinement of the carbon atoms. The disorder for each molecule of CH_2Cl_2 in case (b) is 0.56(2) (C48, Cl3, Cl4) and 0.60(3) (C49, Cl5, Cl6). For case (d), the CH_2Cl_2 carbon and chlorine atoms were refined anisotropically, and the disorder for each molecule of CH_2Cl_2 is 0.46(6) (C48, Cl3, Cl4) and 0.43(1) (C49, Cl5, Cl6). For case (g), one molecule of CH_2Cl_2 [disorder = 0.39(1)] was refined using the ISOR command because unrestrained anisotropic refinement resulted in unstable refinement for the carbon atom. Both molecules of CH_2Cl_2 in **4B**·1.31CH_2Cl_2 were refined

with partial occupancy [0.60(1) for C48, Cl1, Cl2; 0.70(1) for C49, Cl3, Cl4]. Positional disorder throughout **4B**·1.31CH_2Cl_2 and **4H**·1.5CH_2Cl_2 was resolved by applying similar constraints to the thermal parameters.

[$PtCl_2$(TXPB)]·hexane (1B): A solution of [$PtCl_2$(COD)] (52 mg, 1.39 x 10^{-4} mol) and TXPB (100 mg, 1.46 x 10^{-4} mol) in CH_2Cl_2 (10 ml) was stirred at room temperature for 1 hour. The resulting solution was evaporated to dryness *in vacuo* leaving an oily orange solid to which hexanes (15 ml) was added. After sonication for 30 minutes, the mixture was filtered to collect a peach solid which was washed with hexanes (x 1) and dried *in vacuo*. Yield = 78 mg (59 %). **^{1}H NMR (CD_2Cl_2):** δ 7.83 (s, 1H, C*H*^{1}), 7.77 (m, 1H, *Ph*), 7.63-7.59 (broad m, 1H, *Ph*), 7.60 (m, 1H, C*H*^{8}), 7.57-7.48 (m, 3H, *Ph*), 7.38-7.12 (m, 15 H, Ph), 7.25 (d, *J* 11 Hz, 1H, C*H*^{3}), 7.13 (s, C*H*^{6}), 2.17, 1.55 (broad s, 2 x 3H, C*Me*$_2$), 1.25 (s, 9H, C^{2}C*Me*$_3$), 1.17 (s, 9H, C^{7}C*Me*$_3$). **^{13}C{^{1}H} NMR (CD_2Cl_2):** δ 155.05 (s, *C*^{2}CMe_3), 151.58, 149.43 (broad s, C^5 & *ipso*-BPh_2), 151.01 (s, *C*^{7}CMe_3), 150.50 (s, *C*^{12}), 145.84 (d, *J* 12 Hz, *C*^{10}), 140.96 (s, *C*^{13}), 137.86 (s, *C*^{11}), 135.9, 135.2, 134.6, 134.1, 133.0, 132.9, 129.7, 129.2, 127.5, 127.4, 127.4, 126.7 (s, 12 x *Ph*), 133.97 (s, *C*H^6), 131.65 (d, *J* 66 Hz, *C*^{4}), 129.20 (s, *C*H^3), 127.11 (s, *C*H^1), 121.17 (s, *C*H^8), 43.03 (s, *C*Me_2), 35.64 (s, C^2*C*Me_3), 35.28 (s, C^7*C*Me_3), 31.42 (s, 2 x C*Me*$_3$), 28.36, 26.19 (s, 2 x C*Me*$_2$). **^{31}P{^{1}H} (CD_2Cl_2):** δ +32.48 (s, $^1J_{P,195Pt}$ 3836 Hz). **^{11}B (CD_2Cl_2):** δ 3 (broad s). **Anal.** Calcd. for $C_{53}H_{62}PSBCl_2Pt$: C, 61.27; H, 6.01. Found: C, 61.33; H, 5.47 %.

[PtI_2(TXPB)] (4B): A solution of [PdI_2(COD)] (37 mg, 6.64 x 10^{-4} mol) and TXPB (55 mg, 8.01 x 10^{-5} mol) in CH_2Cl_2 (10 ml) was stirred at room temperature for 30 min. The resulting solution was evaporated to dryness *in vacuo* leaving an orange solid to which hexanes (10 ml) was added. After sonication, the mixture was filtered to collect an orange solid which was washed with hexanes and dried *in vacuo*. Yield = 55 mg (73 %). **^{1}H NMR (CD_2Cl_2):** δ 7.84 (s, 1H, C*H*^{1}), 7.78 (d, *J* 2 Hz, 1H, C*H*^{8}), 7.54-7.45 (m, 6H, *p*-P*Ph*$_2$ & *m*-P*Ph*$_2$), 7.43-7.36 (m, 8H, *o*-P*Ph*$_2$ and B*Ph*$_2$), 7.25 (dd, *J* = 9, 2 Hz, 1H, C*H*^{3}), 7.05-6.97 (m, 6H, B*Ph*$_2$), 6.98 (d, *J* 2 Hz, C*H*^{6}), 2.03 (broad s, 6H, C*Me*$_2$), 1.25 (s, 9H, C^{2}C*Me*$_3$),

1.16 (s, 9H, C^7CMe_3). **$^{13}C\{^1H\}$ NMR (CD_2Cl_2):** δ 154.98 (s, C^2CMe_3), 150.26 (s, C^7CMe_3), 146.92 (broad s, C^5), 146.35 (d, *J* 12 Hz, C^{10}), 145.99 (broad s, *ipso*-BPh_2), 143.36 (s, C^{13}), 139.71 (d, *J* 22 Hz, C^{11}), 138.70 (s, BPh_2), 134.95 (d, *J* 11 Hz, *m*-PPh_2), 134.00 (CH^6), 132.30 (d, *J* 61 Hz, *ipso*-PPh_2), 132.23 (s, *p*-PPh_2), 129.64 (s, C^{12}), 129.09 (s, BPh_2), 129.01 (s, CH^3), 128.77 (d, *J* 12 Hz, *m*-PPh_2), 127.41 (s, BPh_2), 126.88 (s, CH^1), 123.41 (s, CH^8), 44.01 (s, CMe_2), 35.58 (s, C^2CMe_3), 35.27 (s, C^7CMe_3), 31.48 (s, C^2CMe_3), 31.40 (s, C^7CMe_3), 27.01 (s, CMe_2). **$^{31}P\{^1H\}$ (CD_2Cl_2):** δ 41.61 ($^1J_{P,195Pt}$ 3517 Hz). **^{11}B (CD_2Cl_2):** δ 50 ppm (broad s). **Anal.** Calcd. for $C_{47}H_{48}PSBI_2Pt$: C, 49.72; H, 4.26. Found: C, 49.43; H, 4.51 %.

TXPH ligand: A 1.81 M solution of *tert*-butyl lithium in pentane (1.8 ml, 3.32 mmol) was added to a solution of TXPBr (1.00 g, 1.66 mmol) in toluene (60 ml) at –78 °C, and the mixture was allowed to warm to room temperature over 12 hours. The resulting yellow solution was cooled to –78 °C and N_2-saturated MeOH (0.2 ml, 4.9 mmol) was added dropwise. After stirring for 10 min. at –78 °C and 20 min. at room temperature, the mixture was evaporated to dryness *in vacuo*. Hexanes (30 ml) was then added, and the mixture was sonicated before filtration to collect a white solid which was washed with hexanes (x1) and evaporated to dryness *in vacuo*. Yield 765 mg (88 %). **^1H NMR (CD_2Cl_2):** δ 7.55 (m, 2H, CH^1 & CH^8), 7.38-7.35 (m, 6H, *o*-PPh_2 and *p*-PPh_2), 7.31 (app. t d, J 7, 2 Hz, 4H, *m*-PPh_2), 7.29 (d, *J* 8 Hz, 1H, CH^5), 7.19 (dd, *J* 8, 2 Hz, 1H, CH^6), 6.72 (dd, *J* 4, 2 Hz, 1H, CH^3), 1.72 (s, 6H, CMe_2), 1.27 (d, $^2J_{H,P}$ 8 Hz, 9H, PMe_3), 1.32 (s, 9H, C^7CMe_3), 1.12 (s, 9H, C^2CMe_3). **$^{13}C\{^1H\}$ NMR (CD_2Cl_2):** δ 150.38 (s, C^7CMe_3), 149.49 (s, C^2CMe_3), 143.03 (s. C^{10}), 142.82 (s, C^{13}), 137.21 (d, *J* 11 Hz, *ipso*-PPh_2), 135.99 (d, *J* 28 Hz, C^{11}), 135.24 (d, *J* 9 Hz, C^4), 134.52 (d, *J* 20 Hz, *m*-PPh_2), 130.34 (d, *J* 9 Hz, C^{12}), 129.4-129.0 (s, *p*-PPh_2 & d, *o*-PPh_2), 128.74 (s, CH^3), 127.52 (s, C^5), 123.69 (s, CH^6), 122.76 (s, CH^1), 121.97 (s, CH^8), 41.50 (s, CMe_2), 35.27 (s, 2 x CMe_3), 31.74 (s, C^7CMe_3), 31.45 (s, C^2CMe_3), 25.32 (s, CMe_2). **$^{31}P\{^1H\}$ (CD_2Cl_2):** δ –8.26 (s). **Anal.** Calcd. for $C_{35}H_{39}PS$: C, 80.42; H, 7.52. Found: C, 80.18; H, 7.50 %.

[$PtCl_2$(TXPH)] (1H): A solution of [$PtCl_2$(COD)] (72 mg, 1.91 x 10^{-4} mol) and TXPH (100 mg, 1.91 x 10^{-4} mol) in CH_2Cl_2 (15 ml) was stirred at room temperature for 1 hour. The resulting yellow solution was evaporated to dryness *in vacuo* leaving a yellow solid to which benzene (15 ml) was added. After sonication, the mixture was filtered to give a pale yellow solid which was washed with benzene and dried *in vacuo*. Yield = 70 mg (43 %). **^{1}H NMR (CD_2Cl_2):** δ 8.78 (d, *J* 8 Hz, 1H, C*H*^{5}), 7.88 (dd, *J* 12, 8 Hz, 2H, *o*-P*Ph*$_2$ A), 7.80 (s, 1H, C*H*^{1}), 7.67 (dd, *J* 13, 8 Hz, 2H, *o*-P*Ph*$_2$ B), 7.64 (s, 1H, C*H*^{8}), 7.63 (t, *J* 8 Hz, 1H, *p*-P*Ph*$_2$ A), 7.56 (app. t, *J* 6 Hz, 2H, *m*-P*Ph*$_2$ A), 7.50 (t, *J* 7 Hz, 1H, *p*-P*Ph*$_2$ B), 7.43 (d, *J* 10 Hz, 1H, C*H*^{6}), 7.40 (d, *J* 9 Hz, 1H, C*H*^{3}), 2.13, 1.74 (s, 2 x 3H, C*Me*$_2$), 1.35, 1.26 (s, 2 x 9H, C*Me*$_3$). **^{13}C{^{1}H} NMR (CD_2Cl_2):** δ 155.45 (d, *J* 7 Hz, *C*^{2}CMe$_3$), 152.78 (s, *C*^{7}CMe$_3$), 146.53 (d, *J* 12 Hz, *C*^{10}), 143.35 (s, *C*^{13}), 139.09 (d, *J* 20 Hz, *C*^{11}), 134.55 (d, *J* 12 Hz, *o*-P*Ph*$_2$ B), 134.43 (d, *J* 11 Hz, *o*-P*Ph*$_2$ A), 132.79 (s, *p*-P*Ph*$_2$ A & B), 131.69 (d, *J* 65 Hz, *C*^{4} or *ipso*-P*Ph*$_2$), 130.22 (s, *C*H^5), 129.49 (d, *J* 12 Hz, *m*-P*Ph*$_2$ A), 129.30 (d, *J* 12 Hz, *m*-P*Ph*$_2$ B), 128.55 (s, *C*H^3), 127.59 (s, *C*H^1), 125.86 (s, *C*^{12}), 125.00 (s, *C*H^6), 123.15 (s, *C*H^8), 43.71 (s, *C*Me$_2$), 35.68 (s, C^2*C*Me$_3$), 35.55 (s, C^7*C*Me$_3$), 31.58 (s, C^{7}C*Me*$_3$), 31.45 (s, C^{2}C*Me*$_3$), 26.56, 26.05 (s, 2 x C*Me*$_2$). **^{31}P{^{1}H} (CD_2Cl_2):** δ +38.60 (s, $^1J_{P,195Pt}$ 3458 Hz). **Anal.** Calcd. for $C_{35}H_{39}PS$: C, 53.30; H, 4.98. Found: C, 53.05; H, 5.27 %.

[$PdCl_2$(TXPH)]·0.5C_6H_6 (2H·0.5C_6H_6): A solution of [$PdCl_2$(COD)] (52 mg, 1.82 x 10^{-4} mol) and TXPH (100 mg, 1.91 x 10^{-4} mol) in CH_2Cl_2 (10 ml) was stirred at room temperature for 1 hour. The resulting orange solution was evaporated to dryness *in vacuo* leaving a bright yellow solid to which benzene (10 ml) was added. After sonication, the mixture was filtered to give a pale yellow solid which was washed with benzene and dried *in vacuo*. Yield = 98 mg (77 %). **^{1}H NMR (C_6D_5Br, 60 °C):** δ 9.38 (d, *J* 7 Hz, 1H, C*H*^{5}), 7.74 (broad s, 5H, C*H*^{1} & *o*-P*Ph*$_2$), 7.53 (s, 1H, C*H*^{8}), 7.29 (s, 1H, C*H*^{3}), 7.14 (m, 3H, C*H*^{6} & *p*-P*Ph*$_2$), 7.04 (broad s, *m*-P*Ph*$_2$), 1.69 (s, 6H, C*Me*$_2$), 1.18 (s, 9H, C^{7}C*Me*$_3$), 1.08 (s, 9H, C^{2}C*Me*$_3$). **^{13}C{^{1}H} NMR (C_6D_5Br, 60 °C):** δ 154.29 (s, *C*^{2}CMe$_3$), 152.82 (s, *C*^{7}CMe$_3$), 146.46 (d, *J* 12 Hz, *C*^{10}), 142.11 (s, *C*^{13}), 137 (*C*^{11}), 133.85 (d, *J* 11 Hz, *o*-P*Ph*$_2$), 131.89 (s, *p*-P*Ph*$_2$), 130.82 (s, *C*H^5), 128.5 (*C*H^3 & *m*-P*Ph*$_2$), 126.40 (s, *C*H^1), 125.23 (s, *C*^{12}), 124.69 (s, *C*H^6), 122.06 (s, *C*H^8), 42.63 (s,

*C*Me$_2$), 34.88 (s, C^2*C*Me$_3$), 34.70 (s, C^7*C*Me$_3$), 31.04 (s, C^{7}C*Me*$_3$), 30.85 (s, C^{2}C*Me*$_3$), 26.60 (s, C*Me*$_2$). **^{31}P{^{1}H} (CD$_2$Cl$_2$):** δ +61.42 (s). **Anal.** Calcd. for $C_{38}H_{42}PSCl_2Pd$: C, 62.77; H, 5.82. Found: C, 63.11; H, 5.67 %.

[RhCl(CO)(TXPH)] (3H): A mixture of [{Rh(μ-Cl)(CO)$_2$}$_2$] (35 mg, 9.00 x 10^{-5} mol) and TXPH (100 mg, 1.91 x 10^{-4} mol) in CH_2Cl_2 (15 ml) was stirred at room temperature for 1 hour. At this temperature, CO was evolved, and the mixture was then warmed to room temperature and stirred for 1 hour. The resulting orange solution was evaporated to dryness *in vacuo* to give an orange solid to which hexanes (15 ml) was added. After sonication, the mixture was filtered to give a mustard yellow solid which was washed with hexanes and dried *in vacuo*. Yield = 98 mg (79 %). **^{1}H NMR (CD$_2$Cl$_2$):** δ 8.85 (d, *J* 8 Hz, 1H, C*H*^{5}), 7.79 (s, 1H, C*H*^{1}), 7.67 (dd, *J* 12, 8 Hz, 4H, *o*-P*Ph*$_2$), 7.62 (s, 1H, C*H*^{8}), 7.50 (t, *J* 7 Hz, 2H, *p*-P*Ph*$_2$), 7.44 (app. t, *J* 8 Hz, 4H, *m*-P*Ph*$_2$), 7.40 (d, *J* 9 Hz, 1H, C*H*^{3}), 7.35 (d, *J* 8 Hz, 1H, C*H*^{6}), 1.86 (s, 6H, C*Me*$_2$), 1.33, 1.24 (s, 2 x 9H, C*Me*$_3$). **^{13}C{^{1}H} NMR (CD$_2$Cl$_2$):** δ 185.99 (dd, $^1J_{C,Rh}$ 78, $^2J_{C,P}$ 16 Hz, Rh*C*O), 153.58 (s, *C*^{2}CMe$_3$), 152.77 (s, *C*^{7}CMe$_3$), 146.11 (d, *J* 13 Hz, *C*^{10}), 143.24 (s, *C*^{13}), 136.85 (d, *J* 27 Hz, *C*^{11}), 134-133 (*C*^{4} & *ipso*-P*Ph*$_2$), 133.57 (d, *J* 12 Hz, *o*-P*Ph*$_2$), 131.70 (s, *p*-P*Ph*$_2$), 129.67 (s, *C*^{5}), 129.39 (d, *J* 11 Hz, *m*-P*Ph*$_2$), 128.33 (s, *C*H^3), 127.33 (s, *C*^{12}), 126.36 (s, *C*H^1), 124.70 (s, *C*H^6), 122.75 (s, *C*H^8), 42.86 (s, *C*Me$_2$), 35.65 (s, C^2*C*Me$_3$), 35.48 (s, C^7*C*Me$_3$), 31.62 (s, C^{7}C*Me*$_3$), 31.49 (s, C^{2}C*Me*$_3$), 25.91 (s, C*Me*$_2$). **^{31}P{^{1}H} (CD$_2$Cl$_2$):** δ +69.52 (d, $^1J_{P,Rh}$ 148 Hz). **Anal.** Calcd. for $C_{36}H_{39}OPSClRh$: C, 62.75; H, 5.70. Found: C, 62.70; H, 5.99 %.

[PtI$_2$(TXPH)]·0.5 toluene (4H·0.5 toluene): A solution of [PtI$_2$(COD)] (128 mg, 2.30 x 10^{-4} mol) and TXPH (120 mg, 2.30 x 10^{-4} mol) in CH_2Cl_2 (10 ml) was stirred at room temperature for 1 hour and then evaporated to dryness *in vacuo*. The residue was then sonicated in toluene (5 ml), and filtered to collect a pale yellow powder. Yield = 141 mg (60 %). **^{1}H NMR (CD$_2$Cl$_2$):** δ 8.66 (d, *J* 8 Hz, 1H, C*H*^{5}), 7.86, 7.70 (v. broad s, 2 x 2H, *o*-P*Ph*$_2$), 7.75 (s, 1H, C*H*^{1}), 7.61 (s, 1H, C*H*^{8}), 7.59, 7.47 (v. broad s, 2 x 1H, *p*-P*Ph*$_2$), 7.49 (v. broad s, 4H, *m*-P*Ph*$_2$), 7.39-7.33 (m, 2H, C*H*^{3} & C*H*^{6}), 2.12, 1.81 (s, 2 x 3H, C*Me*$_2$), 1.34

(s, 9H, C^7CMe_3), 1.22 (s, 9H, C^2CMe_3). **$^{13}C\{^1H\}$ NMR (CD_2Cl_2):** δ 155.50 (s, C^2CMe_3), 153.43 (s, C^7CMe_3), 146.2 (s, C^{10}), 143.58 (s, C^{13}), 139.77 (d, *J* 23 Hz, C^{11}), 134.91 (d, *J* 11 Hz, *o*-P*Ph*$_2$), 133.13 (d, *J* 60 Hz, C^4 or *ipso*-PPh_2), 132.60 (s, *p*-P*Ph*$_2$), 132.36 (s, CH^5), 129.09 (d, *J* 12 Hz, *m*-P*Ph*$_2$), 128.30 (s, CH^3), 127.44 (s, CH^1), 126.01 (s, C^{12}), 124.66 (s, CH^6), 123.28 (s, CH^8), 43.81 (s, CMe_2), 35.62 (s, C^2CMe_3), 35.54 (s, C^7CMe_3), 31.58 (s, C^7CMe_3), 31.46 (s, C^2CMe_3), 26.28 (s, 2 x CMe_2). **$^{31}P\{^1H\}$ (CD_2Cl_2):** δ +47.36 (s, $^1J_{P,195Pt}$ 3249 Hz). **Anal.** Calcd. for $C_{38.5}H_{43}PSI_2Pt$: C, 45.44; H, 4.26. Found: C, 45.45; H, 4.33 %.

DFT Calculations: All structures were fully optimized with the ADF DFT package (SCM, version 2010.02).[39] The adiabatic local density approximation (ALDA) was used for the exchange-correlation kernel[40] and the differentiated static LDA expression was used with Vosko-Wilk-Nusair (VWN) parameterization.[41] All geometry optimizations were conducted using the zero-order regular approximation (ZORA)[42] for relativistic effects, and were gradient corrected using the exchange and correlation functionals of Perdew and Wang (PW91).[43] Geometry optimizations were initially conducted using a double-ζ basis set with one polarization function (DZP) and a medium core, followed by a triple-ζ all-electron basis set with two polarization functions (TZ2P). Crystallographically determined geometries were used as the starting point for calculations on **1B**-**5B**, **2H** and **4H** (for **2B**, the structure from **2B**·$2CH_2Cl_2$ was used). Geometry optimized structures of **1B** and **3B** were used as the starting point for calculations on **1H** and **3H** (after replacement of the BPh_2 group in the TXPB complexes with a hydrogen atom).

Bonding was analyzed in more detail using a fragment approach that considered the interaction of an uncharged MXY [MXY = $PtCl_2$, $PdCl_2$, RhCl(CO), PtI_2 or RhI(CO)] fragment with a neutral TXPB or TXPH ligand (fragments were generated from the TZ2P geometry optimized structures of each complex). Hirshfeld charges,[26] SCF deformation density isosurfaces and Energy Decomposition Analyses[44] were employed to further probe the nature of metal-ligand and boron-halide bonding. Deformation density maps were computed by subtracting the sum of the SCF electron density for the two

fragments (maintained at their optimized positions) from the SCF electron density for the complex. The resulting isosurfaces illustrate the electronic reorganization that occurs upon interaction between the two fragments to form the complex. Mayer bond orders[25,45] were obtained using the ADF keyword EXTENDEDPOPAN. Visualization of the computational results was performed using the ADF-GUI (SCM) or Discovery Studio Visualizer (Accelrys).

Acknowledgement. D.J.H.E. thanks NSERC of Canada for a Discovery Grant, Canada Foundation for Innovation and Ontario Innovation Trust for New Opportunities Grants, and Ontario Centers of Excellence for an Early Researcher Award. B.E.C. thanks the Government of Ontario for an Ontario Graduate Scholarship and NSERC of Canada for a PGS-D award.

Electronic Supplementary Information (ESI) available: Calculated structures for **1B-5B**, **1H-5H**, TXPB and $[TXPB–I]^-$, and X-Ray crystallographic data. See DOI: 10.1039/b000000x/

References

1 (a) A. F. Hill, G. R. Owen, A. J. P. White and D. J. Williams, *Angew. Chem. Int. Ed.*, 1999, **38**, 2759; (b) A. Amgoune and D. Bourissou, *Chem. Commun.*, 2010, 859; (c) G. Bouhadir, A. Amgoune and D. Bourissou, *Adv. Organomet. Chem.*, 2010, **58**, 1; (d) F.-G. Fontaine, J. Boudreau and M. H. Thibault, *Eur. J. Inorg. Chem.*, 2008, 5439.

2 (a) A. J. M. Miller, J. A. Labinger and J. E. Bercaw, *J. Am. Chem. Soc.*, 2008, **130**, 11874; (b) A. J. M. Miller, J. A. Labinger and J. E. Bercaw, *Organometallics*, 2010, **29**, 4499.

3 F.-G. Fontaine and D. Zargarian, *J. Am. Chem. Soc.*, 2004, **126**, 8786.

4 J. Boudreau and F.-G. Fontaine, *Organometallics*, 2011, **30**, 511.

5 I. R. Crossley, A. F. Hill and A. C. Willis, *Organometallics*, 2007, **26**, 3891.

6 (a) K. Pang, J. M. Tanski and G. Parkin, *Chem. Commun.*, 2008, 1008; (b) J. S. Figueroa, J. G. Melnick and G. Parkin, *Inorg. Chem.*, 2006, **45**, 7056.

7 D. J. H. Emslie, J. M. Blackwell, J. F. Britten and L. E. Harrington, *Organometallics*, 2006, **25**, 2412.

8 B. E. Cowie, D. J. H. Emslie, H. A. Jenkins and J. F. Britten, *Inorg. Chem.*, 2010, **49**, 4060.

9 (a) D. J. H. Emslie, L. E. Harrington, H. A. Jenkins, C. M. Robertson and J. F. Britten, *Organometallics*, 2008, **27**, 5317; (b) S. R. Oakley, K. D. Parker, D. J. H. Emslie, I. Vargas-Baca, C. M. Robertson, L. E. Harrington and J. F. Britten, *Organometallics*, 2006, **25**, 5835.

10 A. F. Holleman and E. Wiberg, in *Inorganic Chemistry*. 101st ed.; Academic Press: San Diego, 2001.

11 (a) H. B. Kraatz, H. Jacobsen, T. Ziegler and P. M. Boorman, *Organometallics*, 1993, **12**, 76; (b) N. Taguchi, K. Kashiwabara, K. Nakajima, H. Kawaguchi and K. Tatsumi, *J. Organomet. Chem.*, 1999, **587**, 290.

12 J. M. Zhou, S. J. Lancaster, D. A. Walker, S. Beck, M. Thornton-Pett and M. Bochmann, *J. Am. Chem. Soc.*, 2001, **123**, 223.

13 C. T. Burns, D. S. Stelck, P. J. Shapiro, A. Vij, K. Kunz, G. Kehr, T. Concolino and A. L. Rheingold, *Organometallics*, 1999, **18**, 5432.

14 S. Bontemps, G. Bouhadir, K. Miqueu and D. Bourissou, *J. Am. Chem. Soc.*, 2006, **128**, 12056.

15 S. Bontemps, G. Bouhadir, D. C. Apperley, P. W. Dyer, K. Miqueu and D. Bourissou, *Chem. Asian. J.*, 2009, **4**, 428.

16 J. Vergnaud, T. Ayed, K. Hussein, L. Vendier, M. Grellier, G. Bouhadir, J.-C. Barthelat, S. Sabo-Etienne and D. Bourissou, *Dalton Trans.*, 2007, 2370.

17 (a) T. J. Crevier, B. K. Bennett, J. D. Soper, J. A. Bowman, A. Dehestani, D. A. Hrovat, S. Lovell, W. Kaminsky and J. M. Mayer, *J. Am. Chem. Soc.*, 2001, **123**, 1059; (b) T. J. Crevier and J. M. Mayer, *Angew. Chem. Int. Ed.*, 1998, **37**, 1891.

18 S. J. Lancaster, S. Al-Benna, M. Thornton-Pett and M. Bochmann, *Organometallics*, 2000, **19**, 1599.

19 A. Languérand, S. S. Barnes, G. Bélanger-Chabot, L. Maron, P. Berrouard, P. Audet and F.-G. Fontaine, *Angew. Chem. Int. Ed.*, 2009, **48**, 6695.

20 (a) van der Waals radii: Pt = 1.72 Å, I = 1.98 Å - Bondi, A. *J. Phys. Chem.* **1964**, *68*, 441. (b) Covalent radii : Pt = 1.36, I = 1.39 Å - Cordero, B.; Gómez, V.; Platero-Prats, A. E.; Revés, M.; Echeverría, J.; Cremades, E.; Barragán, F.; Alvarez, S. *Dalton Trans.* **2008**, 2832.

21 M. J. Bayer, T. Muller, W. Losslein, H. Pritzkow and W. Siebert, *Z. Naturforsch. B*, 2004, **59**, 782.

22 D. L. Black and R. C. Taylor, *Acta Crystallogr. B*, 1975, **31**, 1116.

23 G. Canepa, C. D. Brandt and H. Werner, *Organometallics*, 2004, **23**, 1140.

24 A. J. Bard and L. R. Faulkner, in *Electrochemical Methods: Fundamentals and Applications*. 2 ed.; John Wiley & Sons: New York, 2001.

25 A. J. Bridgeman, G. Cavigliasso, L. R. Ireland and J. Rothery, *J. Chem. Soc., Dalton Trans.*, 2001, 2095.

26 (a) F. L. Hirshfeld, *Theor. Chim. Acta*, 1977, **44**, 129; (b) E. R. Davidson and S. Chakravorty, *Theor. Chim. Acta*, 1992, **83**, 319; (c) K. B. Wiberg and P. R. Rablen, *J. Comput. Chem.*, 1993, **14**, 1504; (d) C. F. Guerra, J. W. Handgraaf, E. J. Baerends and F. M. Bickelhaupt, *J. Comput. Chem.*, 2004, **25**, 189; (e) S. Saha, R. K. Roy and P. W. Ayers, *Int. J. Quantum Chem.*, 2009, **109**, 1790.

27 The following bond lengths and angles, Mayer bond orders, Hirshfeld charges, and Energy Decomposition Analysis data were calculated for complex **4B** after geometry optimization with the B–X(1) bond distance constrained to that observed by X-ray crystallography: M–P = 2.243 Å, M–S = 2.276 Å, M–X(1) = 2.690Å, M–Y = 2.641 Å, B–X(1) = 2.758 Å, P–M–X(1) = 173.3°, S–M–Y = 174.0°, M–X(1)–B = 85.9°, Σ(C–B–C) = 349.1°, M–P MBO = 1.175, M–S MBO =

0.979, M–X(1) MBO = 0.734, M–Y MBO = 0.905, B–X(1) MBO = 0.509, M Hirshfeld = 0.0660, X(1) Hirshfeld = –0.0503, X(2) Hirshfeld = –0.1909, B Hirshfeld = 0.0593, MXY Hirshfeld = –0.2713, L Hirshfeld = 0.2718, ΔE_{int} = –462 kJmol^{-1}, ΔE_{orb} = –839 kJmol^{-1}, ΔE_{elec} = –1215 kJmol^{-1}, ΔE_{Pauli} = 1591 kJmol^{-1}.

28 (a) R. J. Thompson and J. C. David, Jr., *Inorg. Chem.*, 1965, **4**, 1464; (b) T. C. Waddington and J. A. White, *J. Chem. Soc.*, 1963, 2701; (c) J. S. Hartman and G. J. Schrobilgen, *Inorg. Chem.*, 1972, **11**, 940.

29 I. Y. Ahmed and C. D. Schmulbach, *Inorg. Chem.*, 1969, **8**, 1411.

30 G. E. Herberich, U. Engerlert, A. Fischer and D. Wiebelhaus, *Eur. J. Inorg. Chem.*, 2004, 4011.

31 K. M. Harmon and F. E. Cummings, *J. Am. Chem. Soc.*, 1965, **87**, 539.

32 (a) P. Jutzi and A. Seufert, *Angew. Chem. Int. Ed. Engl.*, 1977, **16**, 330; (b) P. Jutzi, A. Seufert and W. Buchner, *Chem. Ber.*, 1979, **112**, 2488.

33 N. Wiberg, H. Auer, H. Nöth, J. Knizek and K. Polborn, *Angew. Chem. Int. Ed.*, 1998, **37**, 2869.

34 W. Siebert, *Angew. Chem. Int. Ed.*, 1970, **9**, 734.

35 B. J. Burger and J. E. Bercaw, in Vacuum Line Techniques for Handling Air-Sensitive Organometallic Compounds - Experimental Organometallic Chemistry - A Practicum in Synthesis and Characterization, American Chemical Society: Washington D.C., 1987; vol. 357, pp. 79.

36 A. F. Burchat, J. M. Chong and N. Nielsen, *J. Organomet. Chem.* , 1997, **542**, 281.

37 J. R. Aranzaes, M.-C. Daniel and D. Astruc, *Can. J. Chem.*, 2006, **84**, 288.

38 P. V. D. Sluis and A. L. Spek, *Acta Crystallogr.* , 1990, **A46**, 194.

39 (a) ADF2010, SCM, Theoretical Chemistry, Vrije Universiteit, Amsterdam, The Netherlands, http://www.scm.com. (b) G. te Velde, F. M. Bickelhaupt, S. J. A. van Gisbergen, C. Fonseca Guerra, E. J. Baerends, J. G. Snijders and T. Ziegler, *J. Comput. Chem.*, **2001**, *22*, 931. (c) C.

Fonseca Guerra, J. G. Snijders, G. te Velde and E. J. Baerends, *Theor. Chem. Acc.*, **1998**, *99*, 391.

40 (a) S. J. A. van Gisbergen, J. G. Snijders and E. J. Baerends, *Phys. Rev. Lett.*, 1997, **78**, 3097; (b) S. J. A. van Gisbergen, J. G. Snijders and E. J. Baerends, *J. Chem. Phys.*, 1998, **109**, 10644.

41 S. H. Vosko, L. Wilk and M. Nusair, *Can. J. Phys.*, 1980, **58**, 1200.

42 (a) E. van Lenthe, E. J. Baerends and J. G. Snijders, *J. Chem. Phys.*, 1993, **99**, 4597; (b) E. van Lenthe, E. J. Baerends and J. G. Snijders, *J. Chem. Phys.*, 1994, **101**, 9783; (c) E. van Lenthe, A. Ehlers and E.-J. Baerends, *J. Chem. Phys.*, 1999, **110**, 8943; (d) E. van Lenthe, J. G. Snijders and E. J. Baerends, *J. Chem. Phys.*, 1996, **105**, 6505; (e) E. van Lenthe, R. van Leeuwen, E. J. Baerends and J. G. Snijders, *Int. J. Quantum Chem.*, 1996, **57**, 281.

43 (a) J. P. Perdew, *Phys. Rev. B*, 1986, **33**, 8822; (b) J. P. Perdew and Y. Wang, *Phys. Rev. B*, 1992, **45**, 13244.

44 F. M. Bickelhaupt and E. J. Baerends, in Kohn-Sham Density Functional Theory: Predicting and Understanding Chemistry - Reviews in Computational Chemistry, ed. K. B. Lipkowitz, D. B. Boyd, Wiley-VCH: New York, 2000; vol. 15, pp. 1.

45 (a) Mayer, I. *Chem. Phys. Lett.* **1983**, *97*, 270. Addendum **1985**, *117*, 396. (b) Mayer, I. *Int. J. Quantum Chem.* **1986**, *29*, 73. (c) Sannigrahi, A. B.; Kar, T. *Chem. Phys. Lett.* **1990**, *173*, 569.

Graphical Abstract For Table of Contents Use

Chloro and iodo d^8-metal complexes of the borane-containing TXPB ligand, 2,7-di-*tert*-butyl-5-diphenylboryl-4-diphenylphosphino-9,9-dimethylthioxanthene, and a borane-free analogue, TXPH (2,7-di-*tert*-butyl-4-diphenylphosphino-9,9-dimethylthioxanthene), have been prepared. Analysis of M–X–BR_3 (M = Pd, Pt or Rh; X = Cl or I) bonding in [MX_2(TXPB)] and [MX(CO)(TXPB)] complexes was carried out through the use of crystallographic, spectroscopic, electrochemical and computational comparisons between TXPB and TXPH analogues.